Science Reviews
from the end of the world

Vol. 2, No. 3, October 2023 // pp. 39-51 /

Magnetic nanoparticles for purification of biomolecules: challenges and opportunities

Claudia Rodríguez Torres*[1], Luciana Juncal[1], Elisa De Sousa[1], Odín Vazquez Robaina[1], Natalia Capriotti[2], Karen Salcedo Rodríguez[1], Alberto Nicolás Barrera Illanes[2], Nicolás Mele[1], Carla Layana[2], Lautaro Bracco[3], Juan Pablo Malito[3], Pedro Mendoza Zélis[1], Sheila Ons[2]

[1] *IFLP-CCT-La Plata-CONICET and Departamento de Física, Facultad de Ciencias Exactas, C. C. 67, Universidad Nacional de La Plata, 1900 La Plata, Argentina*
[2] *Laboratorio de Neurobiología de Insectos (LNI), Centro Regional de Estudios Genómicos, Facultad de Ciencias Exactas, Universidad Nacional de La Plata, CENEXA, CONICET, La Plata, Buenos Aires, Argentina*
[3] *INCUINTA, Centro Nacional de Investigaciones Agropecuarias, INTA, Hurlingham, Buenos Aires, Argentina*

** Corresponding author. E-mail: torres@fisica.unlp.edu.ar*

Abstract

The purification and/or concentration of biomolecules from complex mixtures constitutes one of the fundamental steps in the processes involved in biotechnology and, in particular, in the diagnostic methods of human and veterinary diseases. Most purification procedures are based on the interaction between a solid phase and the biomolecule to be purified (RNA, DNA, proteins, etc.), involving several steps with dependence on the method used. Among the different approaches, the use of functionalized magnetic nanoparticles (MNPs) has become of increasing interest due to its efficiency, practicality and the possibility of automation. In this work we present preliminary results on the use of MNPs for the purification of nucleic acids and recombinant proteins.

Keywords: silica coated nanoparticles, nucleic acids, purification methods, recombinant proteins, magnetic nanoparticles

Introduction

In recent decades, the frequency of emerging virus outbreaks has increased, probably as a result of human activity on the environment and the consequent increase in risk of zoonotic transmission. Due to globalization, emerging viruses have a pandemic potential, which has materialized in the case of SARS-CoV2. A pandemic, such as the one experienced, generates an overload of the health systems all over the world, as well as a strong economic and social impact with long-term consequences. Also, climate change has expanded the distribution range of arthropod vectors of pathogenic agents, such as mosquitoes, kissing bugs and ticks. In that context, the inputs for the prevention of the expansion of diseases (diagnosis, treatment and immunization) are scarce globally. Therefore, it is crucial for the sanitary sovereignty of the countries to count with technologies that can allow rapid innovation and national production of supplies for timely diagnosis. In the case of COVID-19, as well as other diseases, although there are certain diagnostic methods that do not require purification of the sample, those more sensitive are based on the identification of viral RNA/DNA by

means of qPCR or isothermal amplifications. For these methods, a purification step of the genetic material is necessary. This purification step is a limitant in the processivity of diagnosis. For this reason, it is necessary to count with robust, high-performance, cost-efficient and locally produced purification methods. This is necessary for the diagnosis of both infectious and genetic diseases, genomics and also in research laboratories.

Currently available commercial kits present a number of drawbacks, such as low throughput in terms of samples per hour, high cost/efficiency ratio, need for specific equipment (such as refrigerated centrifuges), and/or low disponibility in moments of high global demand. Magnetic nanoparticles (MNPs) functionalized in order to efficiently and specifically adsorb biological molecules have aroused growing interest, in view of its low production cost and the possibility of being separated by a magnetic field. Iron oxide MNPs have a large surface area relative to their volume, and offer physicochemical properties that make them ideal candidates for purification in diagnostics and in the pharmaceutical industry, as well as for applications such as immunotherapy, controlled release of drugs (drug delivery), cancer therapy by hyperthermia, etc [1,2]. In particular, the MNPs of iron oxide have a superparamagnetic behavior, which allows the separation of biological molecules adsorbed by applying a magnetic field. This type of particle has been used to adsorb proteins, nucleic acids, lipids, and polysaccharides (reviewed recently in reference [3]).

The purification of recombinant proteins is relevant in a multiplicity of applications, both in the pharmaceutical industry and in biotechnology. For this, the use of labels (tag) of Histidine (His6) in affinity chromatography is a gold standard, and is based on the strong affinity of this sequence by metals such as Ni^{2+}, Cu^{2+}, Zn^{2+} and Co^{2+}. The use of MNPs coated with any of these metals would be a more efficient, fast, economical and sustainable method than chromatography [4, 5].

In this work we present results regarding the efficiency of MNPs for the purification of nucleic acids and preliminary studies using the recombinant anti-Spike-SARS-CoV nanobody protein as a model.

1. Nucleic acid purification

1.1 Synthesis of silica coated magnetite nanoparticles

Magnetic Fe_3O_4 nanoparticles (core, MNPs) were prepared by co-precipitation method from a mixture of $FeCl_2$ and $FeCl_3$ (1:2 molar ration) upon addition of NH_4OH (25% wt) [6]. The resulting black product (bare MNPs) was collected with a magnet and washed several times with deionized water. Subsequently, as-prepared bare MNPs were dispersed in ethanol after 30 minutes of sonication. The reaction mixture was placed in a round bottom flask and ammonium hydroxide solution (25% wt) was added. The SiO_2 functionalization was performed using the protocol provided by [7]. Briefly, SiO_2 functionalization was achieved by the hydrolysis of tetraethyl orthosilicate (TEOS) that was added into the solution mixture dropwise. The mixture was heated up to 80 °C under vigorous magnetic stirring allowing the formation of silica layers on the surface of MNPs. Afterwards, the silica-coated MNPs (MNPs@SiO_2) were collected with a magnet and then washed with ethanol first and then deionized water several times to remove residual TEOS.

1.2 Physico chemical characterization

Several batches of MNPs and MNPs@SiO_2 were prepared following the procedure described above. The quality controls did not show significant differences in the structure and properties of the particles of the different batches, indicating the reproducibility of the method of synthesis. The MNPs@SiO_2 total concentrations (wt/vol) in the colloids were estimated from the weighted mass of dried samples, and the Fe concentration in the samples was determined by means of the so-called thiocyanate method [8]. The silica percentage of microparticles used for nucleic acid purifications is around 40 %. Dynamic light scattering (DLS, Malvern ZetasizerNanoZS) was used to measure the hydrodynamic size and Z-potential at room temperature and $_pH$=7, MNPs@SiO_2 are in water solution. It was determined that they have a hydrodynamic size between 0.8 and 1.2 µm, and a Z potential between -30 and -42 mV. The microstructure of the resulting particles was confirmed by optical microscopy and atomic force microscopy (see Figure 1). A drop of ferrofluid was dried from a microscope slide and observed using a Leica DM IL LED 1000 microscope with a Nikon D3100 camera attached (**Fig. 1a)**. Using ImageJ software, ellipses were drawn manually of 102 particles, and the mean radius of each particle was collected. Mean value and standard deviation were obtained from this set of values, in addition particle size histogram was fitted with a log-normal function **(Fig. 1b)**. A mean diameter of 1.4 µm with a standard deviation (σ) of 0.17 µm was obtained. In **Fig. 1c** is shown a typical topographic AFM image showing one silica coated microparticle and in **Fig. 1d** is shown the cross section along the line indicated in **Fig. 1c**. It can be seen that lateral dimensions are in the order of microns while the normal one is around 300 nm, indicating that the particles had obloid spheroid shapes. A closed inspection also showed that the silica coated microparticles were composed of several bare MNPs.

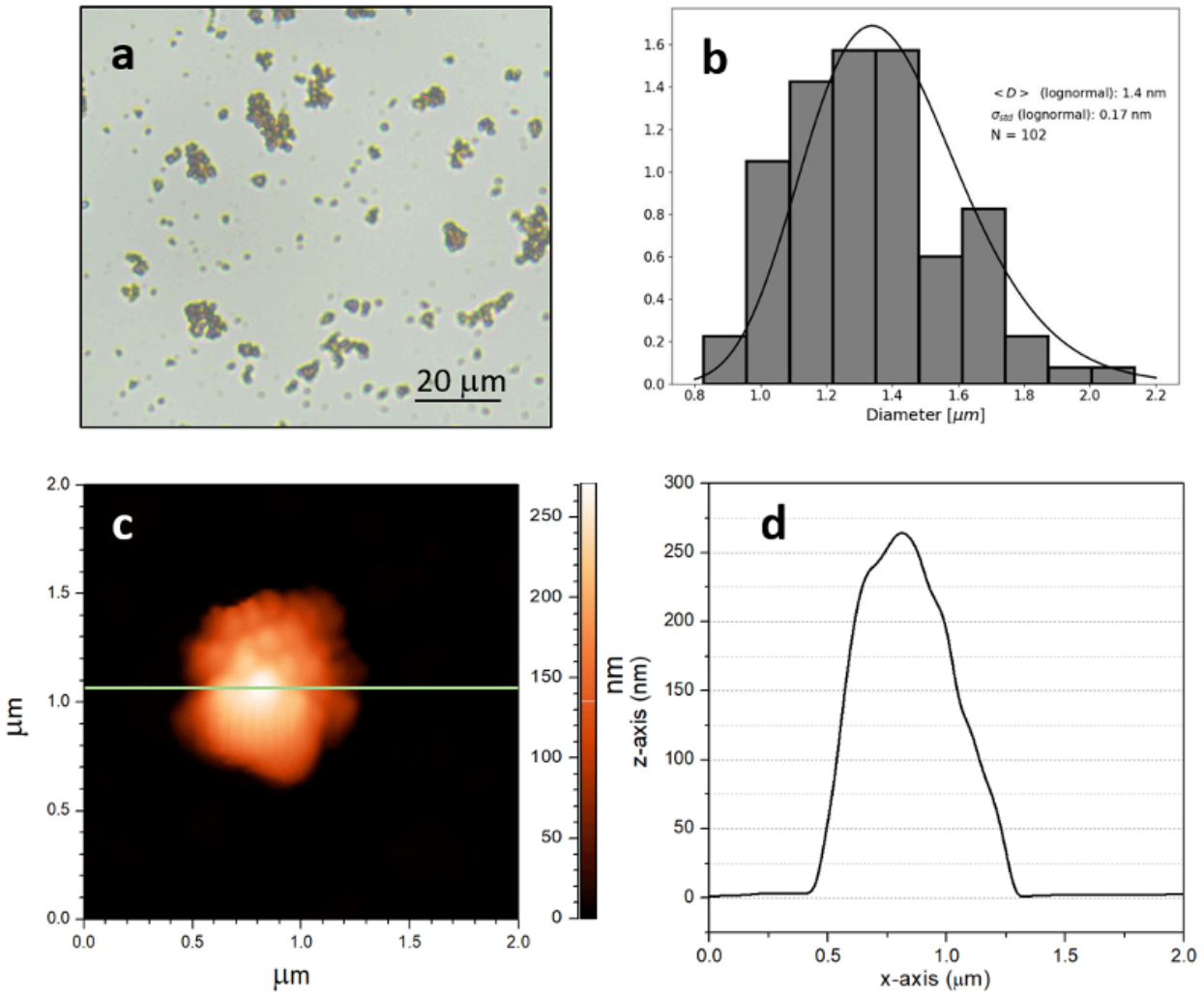

Fig. 1. a) Dried drop of particles of MNPs@SiO_2 observed using a Leica DM IL LED 1000 microscope. **b)** Particle size histogram obtained from image **a)** and the corresponding fit using a log-normal function. **c)** Typical topographic AFM image of one MNPs. **d)** Cross section along the line indicated in **c**.

To evaluate the capture efficiency of MNPs and MNPs@SiO_2 using permanent magnets we measure the force that can be exerted on them when they are exposed to a magnetic field, called magnetic force. In **Fig 2.a** is shown a schematic diagram of the arrangement used to measure magnetic force. The sample is suspended over the center of a $Nd_2Fe_{14}B$ permanent magnet resting on an analytical balance. The attraction force exerted on the magnet by the sample modifies its apparent weight. The experiment was performed using a magnet as used in magnetic racks designed for manual purification. The results are shown in **Fig 2.b.** as the vertical components of magnetic force per unit weight vs. sample-magnet distance. The gray zone represents the working zone in manual extraction experiments, showing that in this region the MNPs are subjected to forces that exceed their weight by at least one order of magnitude, thus ensuring their successful capture. **Fig 2.b.** (inset) shows a zoom corresponding to the region where the magnetic force per unit weight exceeds the unity, a distance that defines the capture region. Any MNP within 14.5 mm will be captured by the magnet allowing an efficient purification ensuring the capture of all the MNP inside the vessel. In **Fig 2.c.** two MNP solutions are shown, one as it is obtained from the synthesis and the other one exposed to a magnet. Additionally, the magnetic properties of bare MNPs and MNPs@SiO_2 samples were investigated using a Lake Shore 7400 vibrating sample magnetometer (VSM). Hysteresis loops were taken at room temperature with a maximum applied field of 1.9 T (**Fig 2.d.**). The saturation magnetization (MS) of MNPs and MNPs@SiO_2 are about 70 and 40 emu/g, respectively while the remanence and coercivity are almost zero in both cases, as expected for the single magnetic domain in the superparamagnetic regime. The nanometer size of the particles results in a single domain structure with superparamagnetic behavior. This characteristic is fundamental for two reasons: it ensures a high magnetic response to small applied fields, while in the absence of field the MNPs do not present a net magnetic moment due to thermal fluctuations avoiding their spontaneous agglomeration and its consequent decantation.

A solution with a concentration of 10 mg/mL was prepared to carry out the extraction tests.

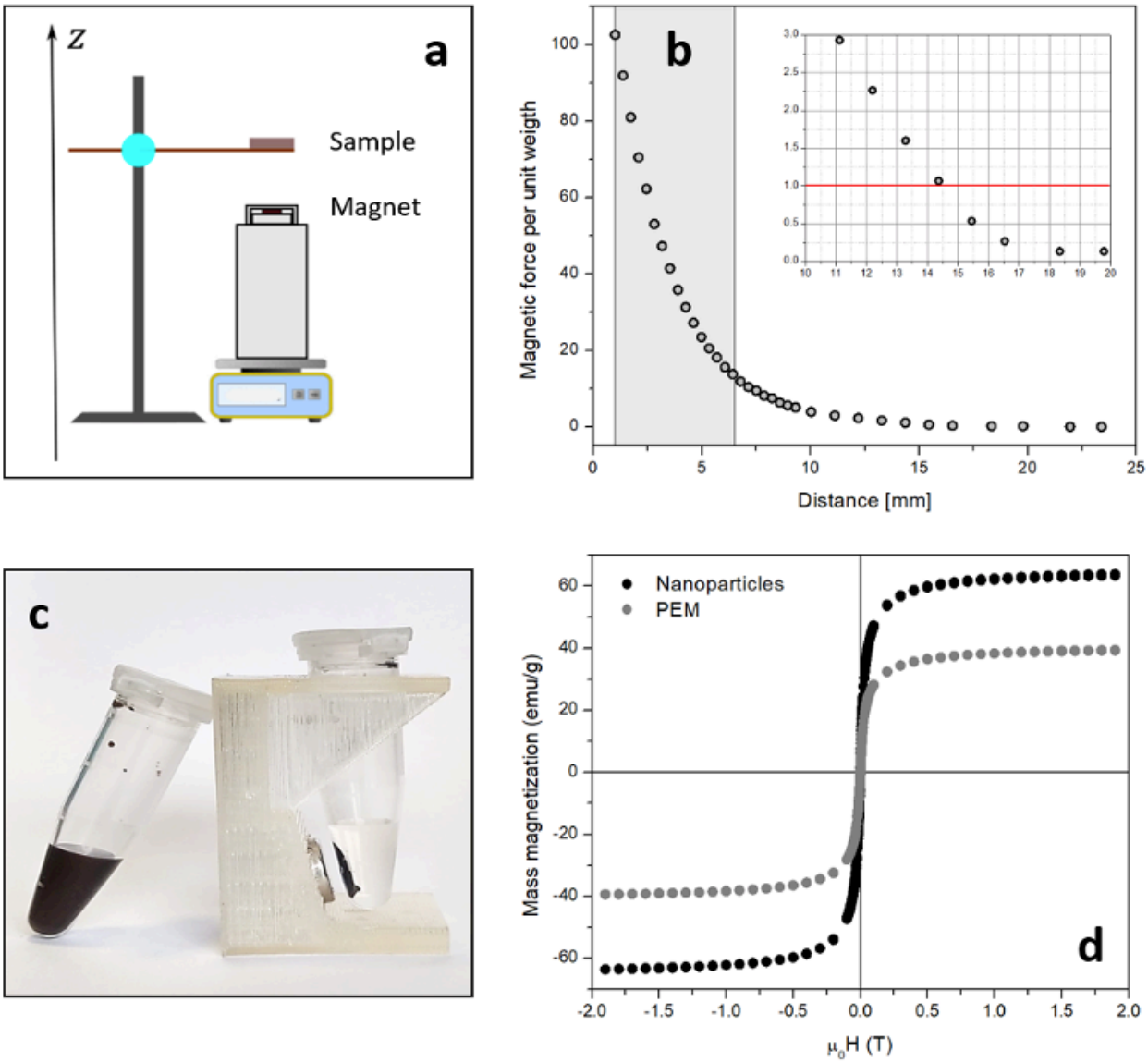

Fig. 2. a) Schematic diagram of the arrangement used to measure magnetic force. **b)** Vertical components of magnetic force per unit weight vs. sample-magnet distance. The gray zone represents the working zone in manual extraction experiments. Inset: detail of the region where the magnetic force per unit weight exceeds the unity (capture region) **c)** Two MNPs solutions, one exposed to the magnetic field generated by the home-made magnetic rack used for manual purification. **d)** Hysteresis loops at room temperature of bare nanoparticles and silica coated nanoparticles.

1.3 RNA purification

In order to assess the performance of MNP@SiO_2 for RNA extraction, we tested a protocol that, briefly, involves a step of biological sample solubilization in a lysis buffer, binding of the MNP with RNA, isopropanol and ethanol washes and resuspension of the purified RNA. Once obtained RNA, the corresponding DNase (PB-L, Productos Biologicos, Argentina) treatment was carried out to eliminate genomic DNA and the subsequent synthesis of the cDNA with the M-MLV (PB-L, Productos Biologicos, Argentina) reverse transcriptase was performed. The samples were used as a template for the detection of a housekeeping gene through the qRT-PCR technique. We assayed this protocol on different insect tissues as biological samples, derived from the insect model *Drosophila melanogaster*, the haematophagous *Rhodnius prolixus* and the phytophagous *Nezara viridula*. Firstly, we evaluate different conditions to optimize the protocol and the

quality of the RNA purified with *D. melanogaster* as biological starting material (pools of 3 insects per treatment) and specific primers for the amplification of tubulin transcript (primer sequences: 5'-TGTCGCGTGTGAAACACTTC-3´ and 5´-AGCAGGCGTTTCCAATCTG-3´). **Fig 3.a.** shows cycle threshold (Ct) values obtained with different concentrations of guanidine isothiocyanate (GITC) in the lysis buffer (2M, 4M and 6M) showing that GITC 4 M gave the better yield, with a mean in Ct value of 21.65±1.23. Also, we compare different detergent compositions in lysis buffer, i.e Triton or Sarkosyl 3% obtaining $Ct_{(Triton)}$ 32.58±1.85 vs. $Ct_{(Sarkosyl)}$ 25.84±2.32 (**Fig 3.b)**. Subsequently, we evaluated if the use of Proteinase K and Ditiotreitol (DTT) in the lysis buffer improved the yield of the purified RNA. Results showed that the addition of either proteinase K or DTT to the lysis buffer did not improve it **(Fig 3.c.).** The MNP methodology was sensitive in the detection by RT-qPCR even for small starting material, such as 0.5 *D. melanogaster*: Ct 28.13±0.68 **(Fig 3.d.)**.

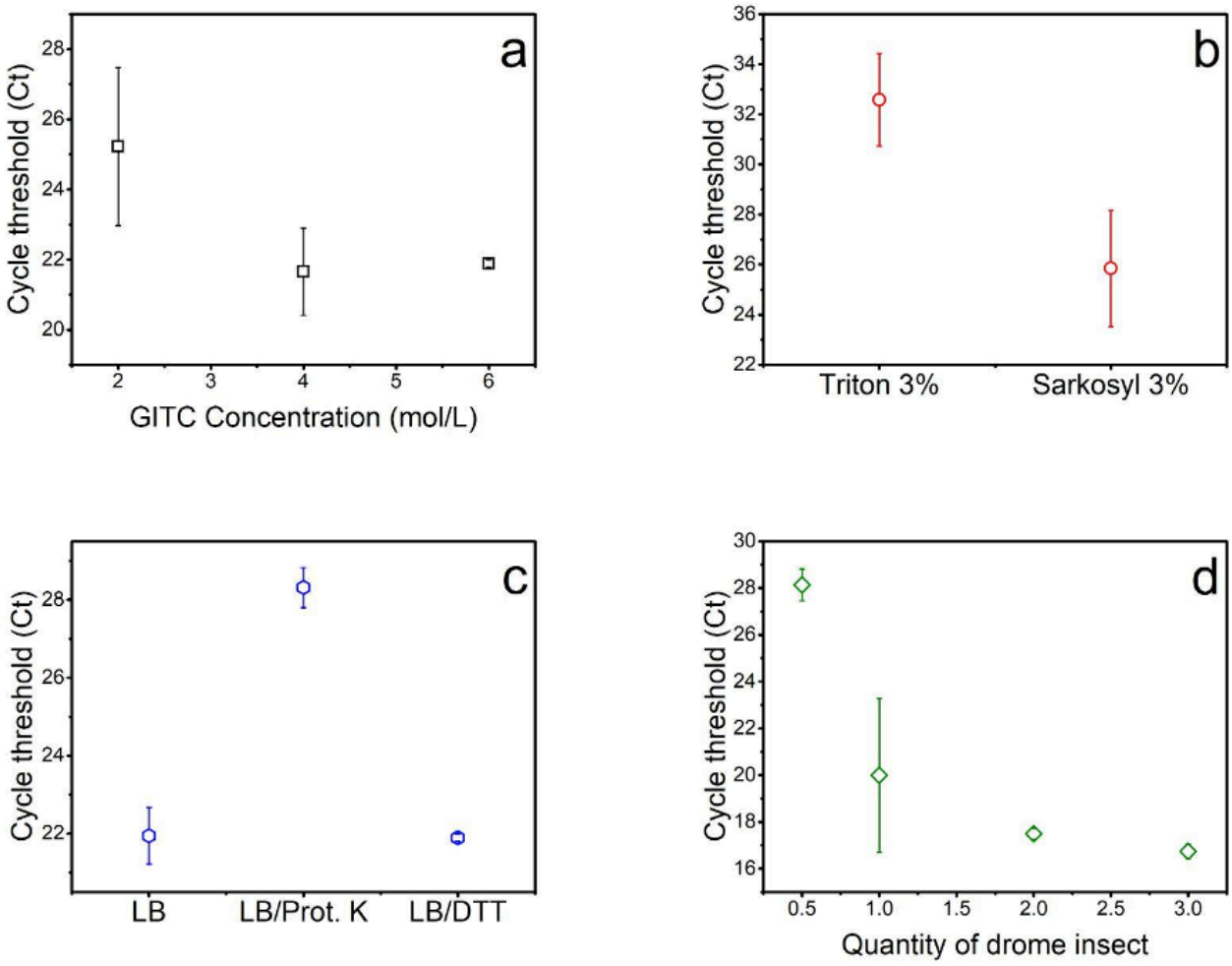

Fig. 3. Performance of MNP in RNA extraction under different conditions.

In the case of *R. prolixus* and *N. viridula*, we dissected one insect per treatment to obtain "soft tissue" (without cuticle). RNA was extracted in parallel with Trizol Reagent (Ambion, USA) following manufacturer instructions and MNP method. We included a step of centrifugation before MNP addition, in order to discard cell debrises that could interfere with the reaction. We obtained amplification of the *Rpro*β- actin gene (primer sequences: 5'-ATCTGTTGGAAGGTGGACAG-3' and 5'-CCATGTACCCAGGTATTGCT-3') and *Nvir*β- actin gene (primer sequences: 5'-CTGTACTCTCCCTCTATGCCTCC-3' and 5'-CACGTCCAGCAAGATCCAG-3') by both methods with similar Ct. As far as NPM protocols were concerned, it was useful for RNA extraction and was useful for use in qPCR detection **(Fig 4).**

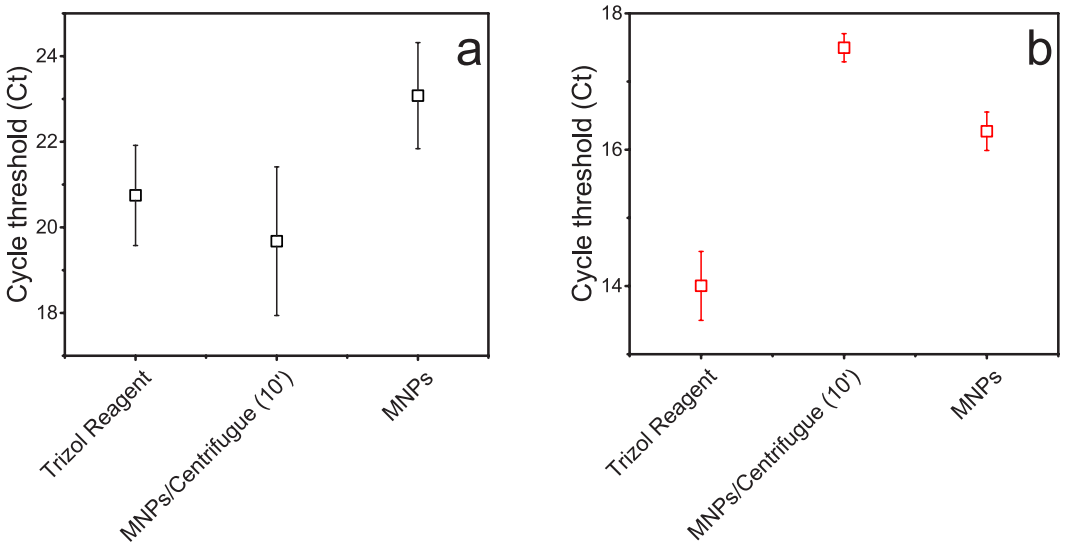

Fig. 4. Comparison of TRIzol reagent and NPM method in RNA purification of **a)** *R. prolixus* and **b)** *N. viridula* "soft tissue".

1.4 DNA purification

For DNA purification, we used a single *Ae. aegypti* mosquito for each replicate (N=3 per treatment). We compared two protocols: one of them using RNAse (DNA protocol), and the other without the use of RNAse (total nucleic acids protocol). In each of them, we also compared 2 Lysis buffer conditions: pH 6 and pH 8. Besides, we used different commercial kits, to compare yield and quality of DNA **(Fig. 5a.)**. We also performed RT-qPCR using primers that amplify on a genomic region of the voltage-gated sodium channel gene (primer sequences: 5'-CAAATTGTTTCCCACTCGCACAG-3' and 5'-AGTAAGTATTCCGTTTGGAAGTTC-3'). We observed that the MNP method, in both protocols and both pH buffer conditions, presented a better performance in terms of lower Ct values, when compared with the three commercial methods. Besides, no difference in Ct values nor DNA yield were observed among the different protocols based on MNPs (**Fig. 5**).

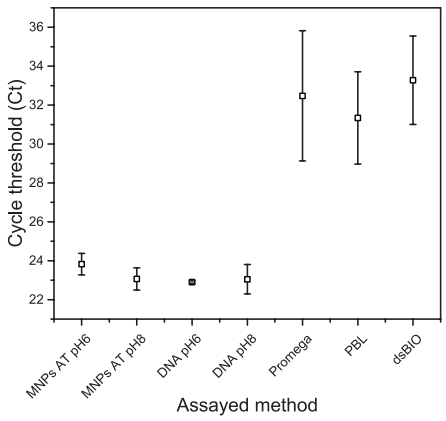

Fig. 5. Comparison of performance in RT-qPCR from different protocols to extract DNA from an *Ae. aegypti* adult mosquito. AT: protocol for total nucleic acids; DNA: protocol for DNA obtention only. Different commercial kits were used.

2. Protein purification

2.1 Synthesis of Ni^{2+} coated magnetite nanoparticles

MNPs were prepared following the synthesis route descriptive in section 1.1. For the following steps a modified route to that reported for [9] and [10] was followed. Briefly, for silica coating, MNPs were magnetically separated and washed with deionized water and dispersed in ethanol. TEOS was added dropwise to the above mentioned mixture. After magnetically stirring at room temperature for 6 h, the product (MNP@SiO_2) was separated and washed with a ethanol and deionized water mixture. Next, the particles were amino-functionalized dispersing MNP@SiO_2 in a mixture of ethanol and water (1:1) and then APTES was added slowly. The solution was heated to 60 ºC with vigorous stirring for 36 h. The final product (MNP@SiO_2@NH_2) was separated by magnetic decantation and washed with deionized water and ethanol. In order to coat the MNP@SiO_2@NH_2 with 2-amino benzamide, MNP@SiO_2@NH_2 were suspended in ethanol and sonicated to form a uniform dispersion. To this mixture isatoic anhydride was added and the resulting mixture was refluxed for 12 h. The prepared functionalized magnetic nanoparticles (MNP@SiO_2@NH_2@AB) were separated magnetically and then washed with ethanol several times to remove unreacted reactives. The last step was the immobilization of nickel. For this purpose, MNP@SiO_2@NH_2@AB particles were ultrasonically dispersed in ethanol and then $NiCl_2.6H_2O$ solution was added. The mixture was refluxed for 12 h. The product (MNP@SiO_2@NH_2@AB@Ni^{2+}) was washed several times with ethanol and dried under vacuum.

2.2 Physicochemical characterization

In order to check the functionalization in the different steps of the synthesis we performed DLS (solution in water), XRD and FT-IR measurements. As can be seen in **Fig 6 (a)** after reaction with TEOS molecules the surface charge of magnetic MNP@SiO_2 nanoparticles is -7.7 ± 0.1 mV which confirms the formation of more OH groups on the surface of MNP. Subsequently, the addition of APTES changed the zeta potential to a more positive value, 3.6 ± 0.1 mV as a result of the increase of amino groups on the surface MNP@SiO_2. The coat with 2-amino benzamide practically does not change the surface charge of MNP@SiO_2@NH_2@AB, 4.7 ± 0.3 mV, in comparison to MNP@SiO_2@NH_2 since each 2-aminobenzamide molecule supplies one amine group. However, the immobilization of Ni^{2+} increases the zeta potential of MNP@SiO_2@NH_2@AB by an order of magnitude which confers stability to the colloidal system.

The XRD patterns (**Fig. 6 (b)**) show that the crystal structure of Fe_3O_4 of bare nanoparticles is preserved for MNP@SiO_2@NH_2 and MNP@SiO2@NH_2@AB@Ni^{2+} after surface modification with TEOS and APTES; also, good crystallinity is achieved. FT-IR spectra of MNP@SiO_2@NH_2 and MNP@SiO_2@NH_2@AB@Ni^{2+} were shown in **Fig. 6 (c)**. The highest intense bands located around 3418 cm^{-1} and 1620 cm^{-1} were assigned to the vibration of OH groups [9]. Also, the absorption peak at 1620 cm^{-1} is overlapped with asymmetric COO– stretching and is related to the N–H bending group [11]. In addition, the band at 3428 cm^{-1} corresponds to the N–H stretching vibration of the -NH_2 group [12]. Furthermore, the bands at 1080 cm^{-1} and 460 cm^{-1} Si-O-Si corresponding to dissymmetric stretching vibration and the Si-O bond bending vibration [13], evidencing the formation of SiO_2 shell over Fe_3O_4 core; while the pronounced peak at 580 cm^{-1} was assigned to Fe-O bond vibration [14]. According to [15] the peak around 1536 cm^{-1} can be assigned to C-N stretching vibrations while the deformation vibration absorption peak of N-H appeared at 1558 cm^{-1} (observed like a shoulder in MNP@SiO_2@NH_2@AB@Ni^{2+} spectrum). As reported by [16], the coupling of APTES group is confirmed by the stretching vibration of C–H at 2865 cm^{-1} and 2923 cm^{-1}. The above confirms the formation of APTES layer over SiO_2 cap. At last, the bands located between 1470–1570 cm^{-1} are attributed to bending motion of the N-H coupled to C-N stretching [17].

The saturation magnetization (see **Fig 6 (d)**) varies depending on the coverage of MNPs being around 60 emu/g for the final product. In all cases remanence and coercivity are almost zero, as expected for the single magnetic domain in the superparamagnetic regime.

Thermogravimetric analysis was performed in a Shimadzu TG-50H Thermogravimetric analyzer, in order to evaluate the coating formation on the surface of the MNP and their thermal stability. **Fig. 6 (e)** shows TGA curves of MNP@SiO_2@NH_2 and MNP@SiO_2@NH_2@AB@Ni^{2+} samples. Bare Fe_3O_4 MNPs showed good thermal stability, and about 7.1% weight loss was observed, which perhaps was due to loss of physically adsorbed water molecules and surface hydroxyl

groups on the Fe_3O_4 particles (not shown here). In the case of MNP@SiO_2@NH_2 NPs (red curve), a 0.4% weight loss can be observed between 30°C and 200 °C and is due to loss of physically adsorbed water molecules on the surface, while the weight loss due to APTES coating (between 200 °C and 800 °C) was about 3.4%. TGA analysis of a sample of MNP@SiO_2@NH_2@AB@Ni^{2+} (blue curve) shows a total weight loss of 7.6% , where around 4.4% is due to 2AB coating.

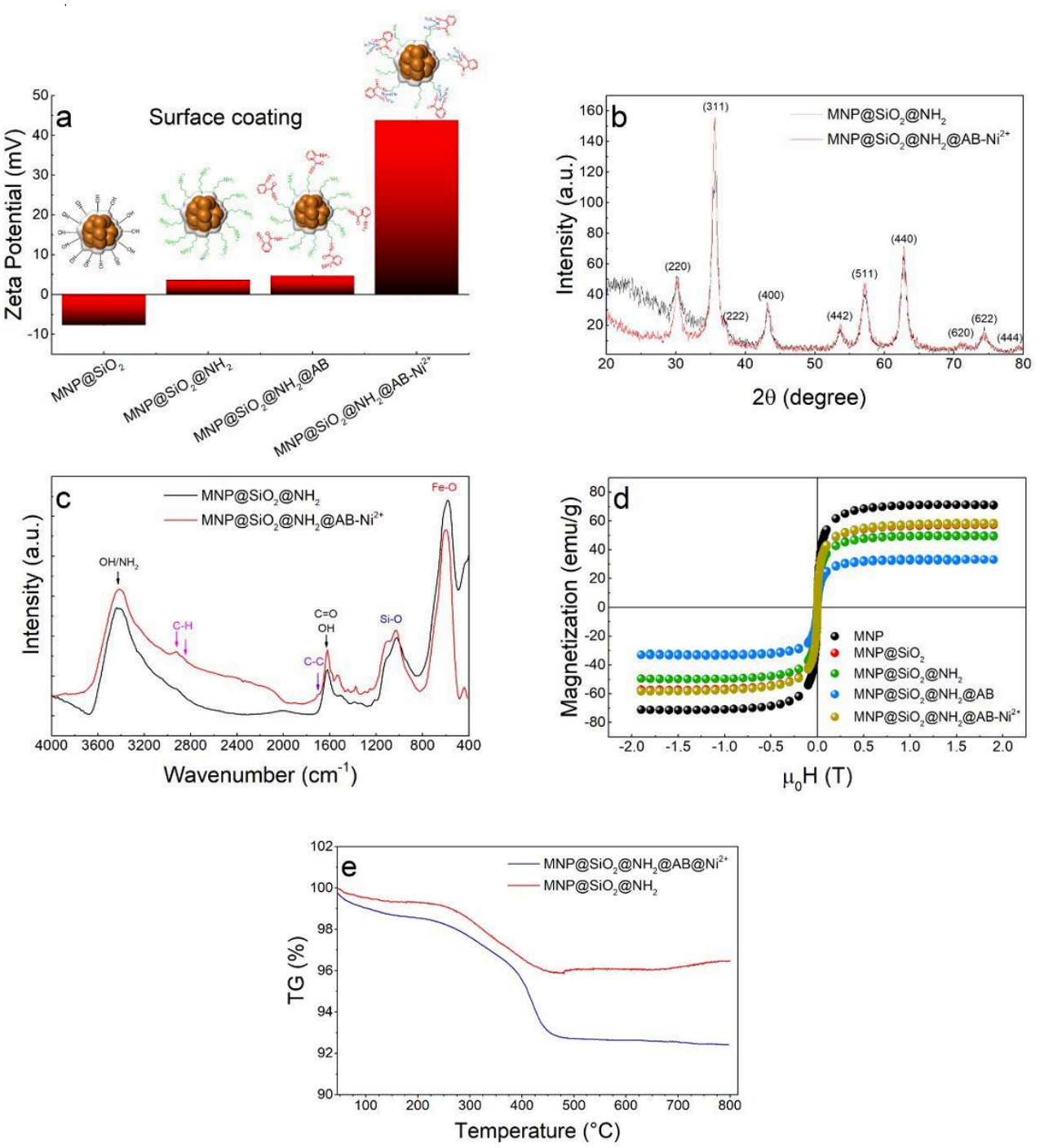

Fig. 6. a) Zeta potential and magnetization curves of microparticles in the different steps of the synthesis. **b)** and **c)** XRD patterns and FT-IR spectra of MNPs@SiO_2@NH_2 and MNPs@SiO_2@NH_2@AB–Ni^{2+}, respectively; **d)** magnetization curves of microparticles depending on the steps of the synthesis. **e)** TGA curves of MNP@SiO_2@NH_2 (red line) and MNP@SiO_2@NH_2@AB@Ni^{2+} (blue line).

The microstructure of the resulting particles were characterized by AFM and SEM measurements. **Fig. 7 (a)** shows the AFM image of a scanned area of 10x10 μm of the NP@SiO_2@NH_2@AB-Ni^{2+} sample and **Fig. 7 (b)** shows the histogram

of the sphere-equivalent particle diameter (D_s), corresponding to 141 particles manually selected in **fig 7 (a)** using the length tool of NT-MDT analysis software. The data was fitted using a log-normal function obtaining a mean value ($<D_s>$) of 272 nm and a standard deviation of 2 nm. Besides, some agglomerates can be observed too, which have a D_s around 250 nm. In **figure 7 (c)** could be observed an individual nanoparticles at lower scan scale area. **Fig. 7 (d)** shows SEM image with the topographic features of an individual nanoparticle.

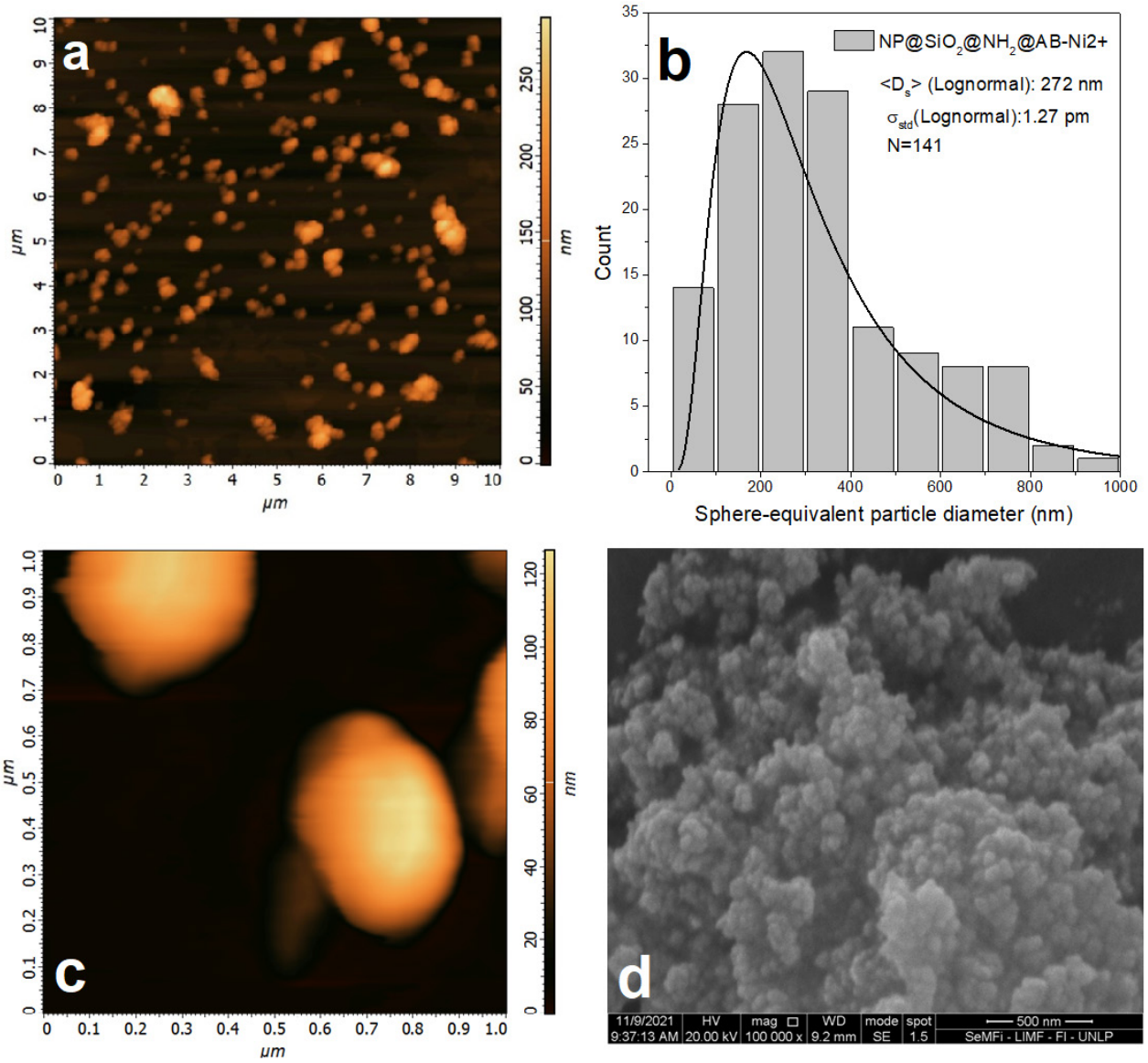

Fig. 7. Topographical analysis of MNP@SiO_2@NH_2@AB-Ni^{2+}: **(a)** AFM image of an overview (10 x 10 μm) sample area. **(b)** Sphere-equivalent particle diameter of the amount of particles observed in (a). **(c)** AFM image of an overview (1 x 1 μm) sample area. **(d)** SEM image obtained from the powder of the sample.

2.3 Protein purification

An anti-Spike-SARS-CoV nanobody derived from llama (Nb39) was expressed in *E. coli* WK6 by transformation using a Phen6 plasmid. After induction with IPTG 1 mM (DO = 0.6), culture was incubated O.N. at 28°C and then harvested by centrifugation at 350 x g for 10 minutes at room temperature. Then, pellet was resuspended in PBS 1X and disrupted using a high-pressure homogenizer Panda 2000 GEA-Niro Soavi, and the cell debris was removed by deep-filtering.

Then, Nb39 was purified using Ni Sepharose™ 6 FF, followed by size exclusion chromatography Sephacryl™ S-100 HR (SEC). Once purified the Nb39 was diluted to a concentration 1,0 mg/mL. On the other hand, MNPs were suspended by sonication in ice for 30 minutes, at 40% power in Washing Buffer (WB: TRIS 20 mM, NaCl 500 mM, Imidazole 20 mM, pH 7.5). MNPs were sonicated in WB for 30 minutes with occasional mixing. Later, 0.17 mL of Nb39 (1.0 mg/mL) were confronted with 0.33 mL of suspended MNPs at the following concentrations: 1 , 2 , 3.75 , 5 or 7.5 mg/mL.

Magnetic separations were carried out for 20 minutes using a GE rack (MagRack6). Pass-through was separated from MNP by pipetting. MNP were then washed twice for 10 minutes using 0.33 mL of WB. Then, the following elution steps were performed (Fig 8a):

1. MNPs were confronted with 85 µL Elution Buffer 1 (TRIS 20 mM, NaCl 500 mM, Imidazole 300 mM, pH 7.5; E1) for 30 minutes at room temperature. After magnetic separation, E1 was removed by pipetting and stored in a clean tube.

2. MNPs were confronted with 83 µL Elution Buffer 2 (TRIS 20 mM, NaCl 500 mM, Imidazole 1000 mM, pH 7.5; E2) for 30 minutes at room temperature. After magnetic separation, E2 was removed by pipetting and stored in a clean tube.

3. MNPs were confronted again with 83 µL Elution Buffer 2 (TRIS 20 mM, NaCl 500 mM, Imidazole 1000 mM, pH 7.5; E2) for 30 minutes at room temperature. After magnetic separation, E2 (duplicate) was removed by pipetting and stored in a clean tube.

Eluted and pass-through fractions were visualized in a polyacrylamide gel electrophoresis stained with coomassie blue (**Fig. 8 b,c**). We observed that the eluted fractions with NMPs contained a notorious amount of 15 kDa Nb39 protein, indeed the elution was better with stronger (1000mM Imidazol, Elution buffer 2) than weaker elution conditions. Also, 2 mg/mL nanoparticles were enough to remove all Nb39 from 1 mg/mL solution, as it is shown in **Fig. 8b**. On the other hand, the amount of MNPs used does not seem to influence the elution performance up to concentrations of 5mg/ml. However, we observed that with high concentrations of NMPs (7.5 mg/ml) no protein is obtained in the eluates. In this case, a high NMPs concentration could make magnetic recuperation and elution difficult. Then, the better condition was 3.75 mg/mL MNPs. These results are a first approach to generate protein purification protocols with these NMPs.

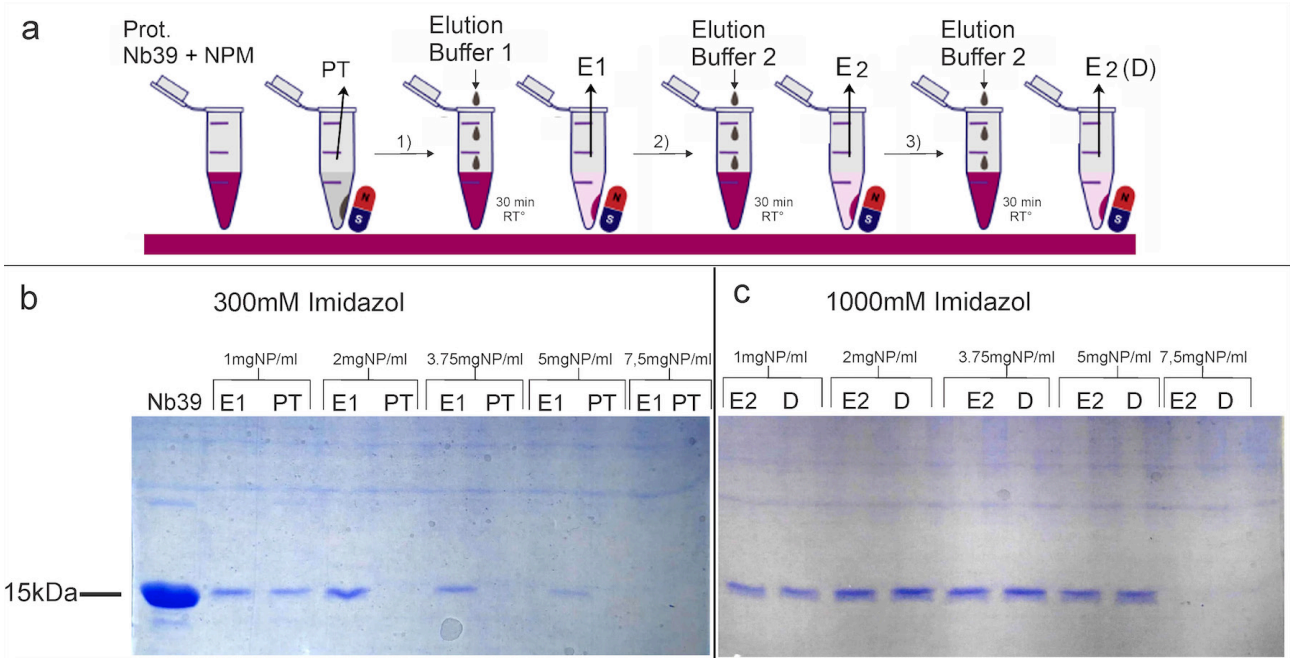

Fig. 8. a) Protein purification protocol. **b,c)** Polyacrylamide gel electrophoresis of eluted and pass-through fractions. **b)** Eluted with Elution Buffer 1, E1: elution PT: Pass-through **c)** Eluted with Elution Buffer 2, E2: elution D: duplicate. Bar size: 15 kDa.

Conclusions

Magnetic separation through nanoparticles plays a promising role in the purification and convenient, selective, and sensitive detection of biomolecules. We present results on the use of functionalized magnetic nanoparticles for the purification of nucleic acids and recombinant proteins. Silica coated magnetic particles synthesized by coprecipitation followed by hydrolysis of tetraethyl orthosilicate were tested for RNA purification on different insect tissues as biological samples, derived from the insect model *Drosophila melanogaster*, the haematophagous *Rhodnius prolixus* and the phytophagous *Nezara viridula* and also for DNA purification from a single adult mosquito of *Ae. aegypti,* vector of dengue disease. Synthesized particles are micrometric size and each microparticle was composed of several bare nanoparticles. Samples presented an appropriate magnetic response maintaining their superparamagnetism properties even after SiO_2 coating. Measurements of magnetic force per unit weight show that in the working zone in manual extraction experiments, magnetic forces exceed MNPs weight by at least one order of magnitude, thus ensuring their successful capture. The results of the purification test show that the obtained coated MNPs are efficient for RNA extraction. We evaluate different conditions of our MNPs based method in order to optimize the protocol, obtaining good qualitative and quantity of RNA. We also observed that for DNA purification, using a single *Ae. aegypti* mosquito, MNPs method using silica coated particles presented a better performance in terms of lower Ct values, when compared with the three commercial methods.

Concerning recombinant proteins purification, we test Ni^{2+} functionalized microparticles synthesized following a chemical route that include several steps in order to obtained silica coated MNPs with 2-aminobenzamide covalently immobilized on their surface to be able to form stable complexes with Ni^{2+} ions. Several experimental techniques were used to check the correct functionalization in each step. The purification assays were performed using anti-Spike-SARS-CoV nanobody derived from llama (Nb39), a 15 kDa recombinant protein expressed and purified from *E. coli* cultures. The results of the purification test show that the MNPs obtained are efficient for total protein extraction from a 1 mg/mL solution of Nb39.

ACKNOWLEDGMENTS

This work was supported with grants from CONICET, AGENCIA I+D+I, and UNLP.

References

[1] Nhiem Tran and Thomas J. Webster, Magnetic nanoparticles: biomedical applications and challenges, J. Mater. Chem., 2010, 20, 8760–8767. DOI: 10.1039/c0jm00994f

[2] Vanessa Fernandes Cardoso, António Francesko, Clarisse Ribeiro, Manuel Bañobre-López, Pedro Martins, Senentxu Lanceros-Mendez, Volume7, Issue5, (2018) 1700845

[3] Abarca-Cabrera, L., Fraga-García, P., Berensmeier, S., 2021. Bio-nano interactions: binding proteins, polysaccharides, lipids and nucleic acids onto magnetic nanoparticles. Biomater. Res. 25, 1–18. https://doi.org/10.1186/s40824-021-00212-y

[4] López-Laguna, H., Voltà-Durán, E., Parladé, E., Villaverde, A., Vázquez, E., Unzueta, U., 2021. Insights on the emerging biotechnology of histidine-rich peptides. Biotechnol. Adv. (2021) https://doi.org/10.1016/j.biotechadv.2021.107817

[5] Jiang, X., Diraviyam, T., Zhang, X., 2016. Affinity purification of egg yolk immunoglobulins (IgY) using a human mycoplasma protein. J. Chromatogr. B Anal. Technol. Biomed. Life Sci. 1012–1013, 37–41. https://doi.org/10.1016/j.jchromb.2016.01.012

[6] De Sousa, M. E., Fernandez van Raap, M. B., Rivas, P. C., Mendoza Zélis, P., Girardin, P., Pasquevich, G. A., Alessandrina, J. L., Muraca, D., & Sánchez, F. H. (2013). Stability and relaxation mechanisms of citric acid coated magnetite nanoparticles for magnetic hyperthermia. The Journal of Physical Chemistry C, 117(10), (2013) 5436-5445. DOI: 10.1021/jp311556b

[7] Oberacker, P., Stepper, P., Bond, D., Hipp, K., Hore, T. A., &Jurkowski, T. P. (2019). Simple Synthesis of Functionalized Paramagnetic Beads for Nucleic Acid Purification and Manipulation. Bio-protocol, 9(20). DOI: 10.21769/BioProtoc.3394

[8] Vogel, A. I., & Jeffery, G. H. (1989). Vogel's textbook of quantitative chemical analysis. Wiley. https://libgen.lc/

edition.php?id=136632479

[9] Rashid, Zahra and Naeimi, Hossein and Zarnani, Amir-Hassan and Nazari, Mahboobeh and Nejadmoghaddam, Mohammad-Reza and Ghahremanzadeh, Ramin, Fast and highly efficient purification of 6×histidine-tagged recombinant proteins by Ni-decorated $MnFe_2O_4$@SiO_2@NH_2@2AB as novel and efficient affinity adsorbent magnetic nanoparticles, RSC Adv., 2016,6, 36840-36848. https://doi.org/10.1039/C5RA25949E

[10] Minkner, R., Xu, J., Takemura, K., Boonyakida, J., Wätzig, H., Park, E.Y., 2020. Ni-modified magnetic nanoparticles for affinity purification of His-tagged proteins from the complex matrix of the silkworm fat body. J. Nanobiotechnology 18, (2020) 1–13. https://doi.org/10.1186/s12951-020-00715-1

[11] Rashid, Z., Naeimi, H., Zarnani, A.-H., Mohammadi, F., & Ghahremanzadeh, R. (2017). Facile fabrication of nickel immobilized on magnetic nanoparticles as an efficient affinity adsorbent for purification of his-tagged protein. Materials Science and Engineering: C, 80, 670–676. doi:10.1016/j.msec.2017.07.014

[12] Yimin, D., Danyang, L., Jiaqi, Z., Shengyun, W., & Yi, Z. (2019). Facile preparation of amidoxime-functionalized Fe_3O_4@SiO_2-g-PAMAM-AO magnetic composites for enhanced adsorption of Pb(II) and Ni(II) from aqueous solution. RSC Advances, 9(16), 9171–9179. doi:10.1039/c9ra00128j

[13] Fang, G., Chen, H., Zhang, Y., & Chen, A. (2016). Immobilization of pectinase onto Fe_3O_4@SiO_2–NH_2 and its activity and stability. International Journal of Biological Macromolecules, 88, 189–195. doi:10.1016/j.ijbiomac.2016.03.059

[14] Shahabi Nejad, M., Seyedi, N., Sheibani, H., & Behzadi, S. (2018). Synthesis and characterization of Ni(II) complex functionalized silica-based magnetic nanocatalyst and its application in C–N and C–C cross-coupling reactions. Molecular Diversity. doi:10.1007/s11030-018-9888-2

[15] Xu, J., Ju, C., Sheng, J., Wang, F., Zhang, Q., Sun, G., & Sun, M. (2013). Synthesis and Characterization of Magnetic Nanoparticles and Its Application in Lipase Immobilization. Bulletin of the Korean Chemical Society, 34(8), 2408–2412. doi:10.5012/bkcs.2013.34.8.2408

[16] Abbas, M. (2014). Fe3O4/SiO2 Core/Shell Nanocubes: Novel Coating Approach with Tunable Silica Thickness and Enhancement in Stability and Biocompatibility. Journal of Nanomedicine & Nanotechnology, 05(06). doi:10.4172/2157-7439.1000244.

[17] Hayashi, T., & Mukamel, S. (2007). Vibrational−Exciton Couplings for the Amide I, II, III, and A Modes of Peptides. The Journal of Physical Chemistry B, 111(37), 11032–11046. doi:10.1021/jp070369b

Bios

Claudia Rodríguez Torres

Bachelor of Physics from the Faculty of Exact Sciences, UNLP. PhD in Physics with a focus on Hard Ferromagnets. She conducted postdoctoral research on the topic of Recrystallization of Cold-Rolled Steels. Currently, she is a Principal Researcher at CONICET (National Scientific and Technical Research Council) and a Professor in the Department of Physics at the National University of La Plata. She is responsible for the Magnetism in Oxides (MagOx) group at the Institute of Physics La Plata and the Thin Film Growth Laboratory (IFLP). Her research area covers topics in solid-state physics, such as semiconductor physics, magnetism, and nanotechnology. Her current main focus is the exploration and design of new materials for spintronics, catalysis, and biotechnology applications. In the context of the COVID-19 pandemic, she led a research project for the development of a viral RNA extraction kit based on magnetic nanoparticles. This project led to the creation of a technology-based company called Magnolia Nanotech SA, of which she is a co-founder.